TECHNICAL RESEARCH REPORT

Institute for Systems Research

Local Nonlinear Control of Stall Inception in Axial Flow Compressors

by R.A. Adomaitis and E.H. Abed

The Institute for Systems Research is supported by the National Science Foundation Engineering Research Center Program (NSFD CD 8803012), Industry and the University

TR 93-40

AIAA 93-2230

Local Nonlinear Control of Stall Inception in Axial Flow Compressors

R. A. Adomaitis and E. H. Abed
Institute for Systems Research
University of Maryland
College Park, MD 20742

AIAA/SAE/ASME/ASEE
29th Joint Propulsion Conference and Exhibit
June 28-30, 1993 / Monterey, CA

LOCAL NONLINEAR CONTROL OF STALL INCEPTION IN AXIAL FLOW COMPRESSORS

Raymond A. Adomaitis and Eyad H. Abed
Institute for Systems Research
University of Maryland
College Park, MD 20742

Abstract

A combination of theoretical and computational nonlinear analysis techniques are used to study the scenario of bifurcations responsible for the initiation of rotating stall in an axial flow compressor model. It is found that viscosity tends to damp higher-frequency modes and so results in a sequence of bifurcations along the uniform-flow solution branch to stall cells of different mode number. Lower-mode stalled flow solutions are born in subcritical bifurcations, meaning that these equilibria will be unstable for small amplitudes. Secondary bifurcations, however, can render them stable, leading to hysteresis. Using throttle position as a control, we find that while the stall bifurcations are not linearly stabilizable, nonlinear state feedback of the first mode amplitude will reduce the hysteresis. This improves the nonlinear stability of the compression system near the stall margin.

1. Nomenclature

a_n, b_n, A_n	mode amplitude coefficients
B	plenum/compressor volume
c	wave speed
f	axisymmetric compressor characteristic
f_0	shut-off head
F	throttle characteristic
H	pressure rise scaling factor
k	controller gain
l_c	overall compressor length
m	exit duct length factor
n	mode number
u	control input
v	axial velocity perturbation
v_0	perturbation at $\eta = 0$
V	mean axial velocity
V_{loc}	total local axial velocity
w	mean velocity scaling factor
α	internal compressor lag
γ	throttle opening
γ_0	nominal throttle opening
Δ_p	plenum-atmosphere pressure rise
η	axial coordinate
θ	circumferential coordinate
λ_n	n'th eigenvalue
μ	viscosity
τ	time

2. Introduction

There are great incentives for understanding the transitions to fully developed rotating stall and developing active control schemes for suppressing the onset of stall. Cast in terms of a bifurcation problem, progress has been made in clarifying the complicated transition scenarios of qualitatively-different flow patterns, both in low-order models[1] and with highly truncated discretizations of distributed parameter models which account for the spatial nature of the stall cells[2]. In parallel with this theoretical work, experimental studies of stall suppression[3]–[5] and numerical analysis of stall avoidance[6] have shown that the range and operability of compressors near peak pressure rise can be improved. This paper combines a more detailed analysis of the transitions to rotating stall with a theoretical and numerical bifurcation study of nonlinear controllers designed to improve the operability of an axial flow compressor operated near peak pressure rise conditions.

Our work begins with a modification to the Moore-Greitzer[7] model to include viscous dissipative forces in the unsteady performance of a compressor blade row. The resulting compression system model, while somewhat more complicated than the original Moore-Greitzer model, is still amenable to formal local stability and bifurcation analysis. Linearization of the axial flow disturbance partial differential equation along the branch of uniform-flow solutions (the axisymmetric compressor characteristic) reveals a countable sequence of bifurcation points. These points mark where nonuniform flow solution branches of different mode numbers are born. The physical interpretation of this phenomenon is that a single cell

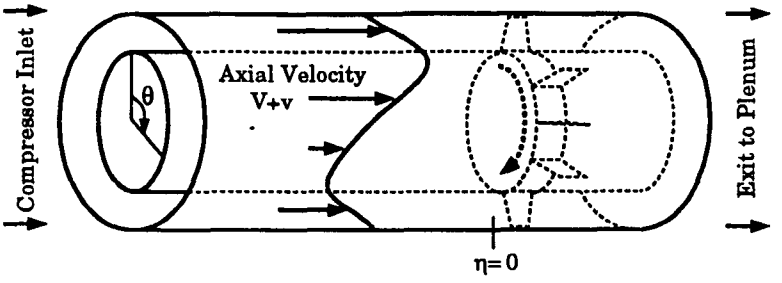

Figure 1: The compressor geometry.

stalled-flow solution is born first and just to the left of the compressor characteristic peak, and stalled-flow solutions of different mode numbers branch off still farther to the left (towards decreasing mean flow values). Substituting the eigenfunction associated with the bifurcating eigenvalue into the flow disturbance PDE and evaluating the mode amplitude coefficient with Galerkin's method, we find the first to be a *subcritical* bifurcation, meaning that the bifurcating solution will be born unstable, and so small amplitude rotating stall cells will not be observed in an actual compression system corresponding to the parameters used in this work.

The practical importance of the subcritical stall bifurcation, however, is that when the uniform-flow operating point becomes unstable to infinitesimal perturbations, the system will jump to a large amplitude, fully developed stall cell. Subcritical bifurcations also imply hysteresis, and so returning the throttle to its original position may not bring the system out of stall. These features are *quantified* with non-local numerical bifurcation analysis and continuation techniques. The points where numerical continuation of the different stalled-flow equilibria are started are determined by the local analysis discussed above. These computations reveal rich sequences of secondary bifurcations, the primary importance of which is they give rise to regions of throttle opening parameter values where fully developed *stable* stalled-flow solutions of different mode number coexist, a phenomenon that has been observed experimentally[8].

Having achieved this basic understanding of the local and global bifurcations associated with rotating stall, we turn to the design and analysis of active control schemes to allow safe operation of the compressor near conditions of peak pressure rise. Building on the work of Liaw and Abed[9], we design output feedback controllers that render the local bifurcations leading to rotating stall supercritical, i.e., stable. Moreover, the ability of such a control law to also limit the amplitude of the bifurcated solution branches over a given parameter range is also studied. These control laws are found to reduce hysteresis effects which occur in the uncontrolled system. Using the throttle opening as a control, it has been shown that the critical eigenvalue is unaffected by linear feedback, and so a quadratic feedback control law using the measurement of the amplitude of the first mode of the axial flow disturbance, or of the pressure rise, is used. This effectively stabilizes the small amplitude stall cells and so reduces the dangerous hysteresis. Bifurcation analysis of a high-order spectral discretization of the full system is used to judge the benefits of the controller.

3. The Compression System Model

3.1. Equations of Motion

A local momentum balance describing the two-dimensional flow in the compressor and its associated ducting (Fig. 1) gives the partial differential equation:

$$\Delta_p = f(V+v_0) - l_C\frac{dV}{d\tau} - m\frac{\partial}{\partial\tau}\int_{-\infty}^{0} v\,d\eta - \frac{1}{2\alpha}\left[2\frac{\partial v_0}{\partial\tau} + \frac{\partial v_0}{\partial\theta}\right]. \qquad (1)$$

Note that our notation differs considerably from the original notation of Moore and Greitzer[7]: V denotes the annulus-averaged (mean) gas axial velocity; v_0 is the axial velocity perturbation evaluated at $\eta = 0$ (the inlet face of the compressor); Δ_p is the plenum-to-atmosphere pressure rise; and η, θ are the axial and angular coordinates.

The compressor pressure rise $f(V_{loc})$ is particular to each compressor and is obtained from experiments in the stable operating range and estimated in the nonuniform-flow range. Following Moore and Greitzer[7], we use a cubic equation in axial velocity

$$f(V_{loc}) = f_0 + H\left[1 + \frac{3}{2}\left(\frac{V_{loc}}{w} - 1\right) - \frac{1}{2}\left(\frac{V_{loc}}{w} - 1\right)^3\right]$$

where $V_{loc} = V + v_0$ (the total local axial flow) and the characteristic parameters used throughout this work

Param	*Value*	*Description*
α	1/3.5	internal compressor lag
l_c	8.0	overall compressor length
m	1.75	exit duct length factor
H	0.18	pressure rise scaling factor
w	0.25	mean velocity scaling factor
f_0	0.3	shut-off head
B	0.5	plenum/compressor volume ratio

Table 1: Values of compressor parameters used in this work.

are given in Table 1, with l_c fixed at a representative value[7],[10].

If the momentum balance (1) is averaged over the circumferential coordinate, we find

$$l_C \frac{dV}{d\tau} + \Delta_p(\tau) = \frac{1}{2\pi} \int_0^{2\pi} f d\theta \tag{2}$$

which can be thought of as determining the amplitude of the zeroth-order Fourier mode, and so (2) determines the transient behavior of the mean flow (V). If there are no spatial variations of gas density and pressure in the plenum, an overall material balance on the gas over the plenum gives:

$$l_C \frac{d\Delta_p}{d\tau} = \frac{1}{4B^2} \left[V(\tau) - F^{-1}(\Delta_p) \right] \tag{3}$$

where the throttle characteristic is given by the orifice equation $F^{-1}(\Delta_p) = \gamma\sqrt{\Delta_p}$. The parameter γ is proportional to the throttle opening.

4. Onset of Stall—Open Loop

Equilibrium solutions to (1-3) which have no spatial variations in the axial velocity profile are the *uniform-flow* solutions. From (2) we obtain

$$\Delta_p = f(V)$$

and from (3)

$$V = \gamma\sqrt{\Delta_p}$$

and so uniform-flow solutions $(\hat{V}, \hat{\Delta}_p)$ are found at the intersections of the axisymmetric compressor and throttle characteristic curves.

If $v_0 = 0$, it can be seen from (1) that the time derivatives of v_0 must remain zero. Thus, computing the two eigenvalues of (2-3) linearized at $(\hat{V}, \hat{\Delta}_p, v_0 = 0)$ will only reveal the stability with respect to perturbations in the mean flow and pressure rise. While this will signal the *local* onset of compressor surge, we must consider perturbations to the spatial flow profile for a complete local stability picture.

4.1. Linearized Stability Analysis

Substituting the annulus-averaged momentum balance (2) into the local momentum balance (1) and linearizing at $V = \hat{V}$ and $v_0 = 0$, we find

$$0 = \frac{df(\hat{V})}{dV} v_0 - m\frac{\partial}{\partial\tau} \int_{-\infty}^{0} v d\eta - \frac{1}{2\alpha} \left[2\frac{\partial v_0}{\partial\tau} + \frac{\partial v_0}{\partial\theta} \right]. \tag{4}$$

Solutions to (4) are linear combinations of functions which are periodic in the circumferential coordinate θ, satisfy $v_0 = 0$ at the inlet duct entrance (at $\eta \to -\infty$), and satisfy the continuity condition (since we assume potential flow in the ducting). These functions are

$$v_n = z_n \exp(\lambda_n \tau + n\eta + in\theta) \tag{5}$$

where z_n is complex and n is the mode number. Substituting (5) into (4) and solving for the eigenvalues λ_n, we obtain

$$\left[\frac{m}{n} + \frac{1}{\alpha} \right] \lambda_n = \frac{df(\hat{V})}{dV} \pm i\frac{n}{2\alpha} \tag{6}$$

and so, as pointed out by Paduano and co-workers[3], the uniform flow solution becomes unstable to spatial perturbations at the peak of the compressor characteristic.

4.2. Bifurcating Stall Cells

The rotating stall equilibria born at the stall bifurcation point are spatial waves of local axial velocity, rotating at a constant speed around the annulus. Near the bifurcation point, the amplitude of the bifurcating mode will dominate the shape of the stall cell. Thus, in the neighborhood of the bifurcation point we can approximate v by the eigenfunction associated with the critical eigenvalue λ_n

$$v = \exp(n\eta) \left[a_n \cos(n\theta) + b_n \sin(n\theta) \right] \tag{7}$$

(so $v_0 = a_n \cos(n\theta) + a_n \sin(n\theta)$). Substituting (7) into (1) to form the residual and using Galerkin's method to determine the amplitude coefficients gives a family (dependent on the stall mode number n) of sets of four ordinary differential equations in time[11].

By introducing the rotating coordinate frame $\theta \mapsto \theta + c\tau$ into the mode amplitude differential equations, the wave speed c of the bifurcating modes can be computed by the requirement that if the coordinates rotate in the amplitude coefficient space at the same speed as the traveling wave, the eigenvalues will cross the imaginary axis *on* the real axis. This requirement gives an explicit expression for the wave speed (c.f. equation (57) of Moore and Greitzer[7]):

$$c = \frac{-n}{2(\alpha m + n)}.$$

Constraining the Fourier mode amplitude coefficients by $A_n^2 = a_n^2 + b_n^2$ gives

$$\frac{m\alpha + n}{n\alpha}\frac{dA_n}{d\tau} = \frac{3HV(2w-V)}{2w^3}A_n - \frac{3H}{8w^3}A_n^3 \quad (8)$$

$$l_C\frac{dV}{d\tau} = -\Delta_p + f_0 + \frac{HV^2(3w-V)}{2w^3} + \frac{3H(w-V)}{4w^3}A_n^2 \quad (9)$$

$$l_C\frac{d\Delta_p}{d\tau} = \frac{1}{4B^2}\left[V - \gamma\sqrt{\Delta_p}\right]. \quad (10)$$

The amplitude of the bifurcating traveling wave comes from the steady-state form of (8) with $A_n \neq 0$:

$$A_n^2 = \frac{8w^3}{3H}\frac{df}{dV}. \quad (11)$$

The steady mean flow V can now be computed from (9)

$$\Delta_p = \left(\frac{V}{\gamma}\right)^2 = \frac{1}{2\pi}\int_0^{2\pi} f d\theta = f_0 + \frac{HV^2(3w-V)}{2w^3} + \frac{3H(w-V)}{4w^3}A_n^2.$$

For $A_n \neq 0$, the mean gas velocity V of the stalled-flow solutions are defined by the cubic polynomial in V:

$$f_0 - \left(\frac{V}{\gamma}\right)^2 - \frac{15HV^2}{2w^2} + \frac{5HV^3}{2w^3} + \frac{6HV}{w} = 0. \quad (12)$$

We must be careful in interpreting solutions to (12), since some of the roots, when substituted back into (11), will give $A_n^2 < 0$, clearly an impossible physical result. Thus, when the physically-relevant roots of (12) are used to compute the axial velocity perturbation amplitude of the bifurcating stalled-flow solutions, and the local stability of the solutions are determined by computing the eigenvalues of the linearization of (8-10), we obtain the bifurcation diagram Fig. 2. In this diagram, solid curves represent locally asymptotically stable solutions and dashed curves indicate unstable solutions.

These results for $n = 1$ have been discussed extensively in the literature[7],[10]. However, from (11) and (12), we observe that both the amplitude of the bifurcating traveling waves and the mean flow and pressure rise are the same for all mode numbers n. Because n can be arbitrarily large, this does not appear to be physically realistic since the large velocity gradients associated with stalled flows of very high cell number will be damped by viscous effects. The addition of a viscous momentum transport term will change the form of (1) and so we should expect important changes in the bifurcation behavior of the modified model.

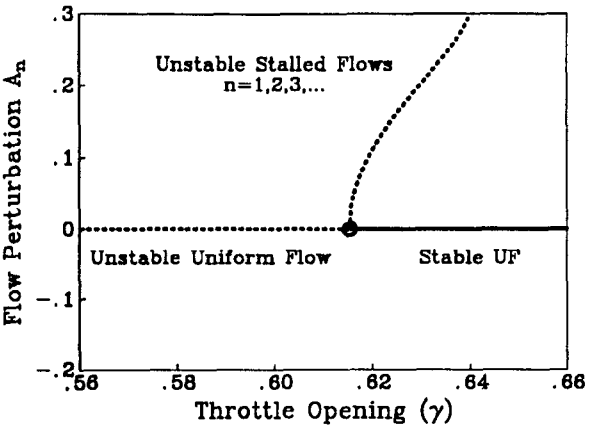

Figure 2: Subcritically bifurcating stall cells.

4.3. Viscous Dissipation

If we include a term which accounts for viscous transport of momentum in the compressor section, (1) becomes

$$\Delta_p = f(V + v_0) - l_C\frac{dV}{d\tau} - m\frac{\partial}{\partial\tau}\int_{-\infty}^{0} v d\eta - \frac{1}{2\alpha}\left[2\frac{\partial v_0}{\partial\tau} + \frac{\partial v_0}{\partial\theta} - \mu\frac{\partial^2 v_0}{\partial\theta^2}\right]. \quad (13)$$

Linearized stability analysis reveals the important difference in the structure of the stall bifurcation—the eigenvalues are now

$$\left[\frac{m}{n} + \frac{1}{\alpha}\right]\lambda_n = \frac{df(\hat{V})}{dV} - \mu\frac{n^2}{2\alpha} \pm i\frac{n}{2\alpha}. \quad (14)$$

This expression can be given some physical "feel" by considering its behavior for very small (positive) μ. For all μ and all mode numbers n, the real part of the eigenvalue expression will be negative for compressor characteristic segments where the derivative of the characteristic with respect to the mean flow V is negative (see the right-most portion of the uniform-flow solution branch in Fig. 3). As the throttle is closed (moving left on the solution branch), the local maximum is crossed and so the derivative changes sign. This means, for small μ and the first stall mode ($n = 1$), the real part of the eigenvalue vanishes at a point just to the left of the peak. Since this point will move farther down (to the left) the uniform-flow branch as the viscosity parameter increases, we see, true to what we should expect, that viscous effects tend to damp out spatial perturbations. Similar arguments can be made for the higher mode (n) bifurcation points shown in Fig. 3.

Another important effect is that the number of bifurcating modes will be reduced from an infinite number (for $\mu \to 0$) to a finite number for $\mu \neq 0$ and for

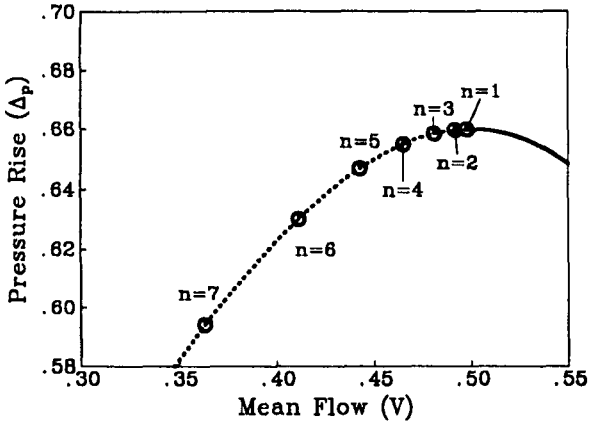

Figure 3: A portion of the uniform-flow solution branch in the uniform-flow phase space (parameterized by throttle opening γ) for $\mu = 0.01$. Circles represent bifurcation points corresponding to different mode numbers n.

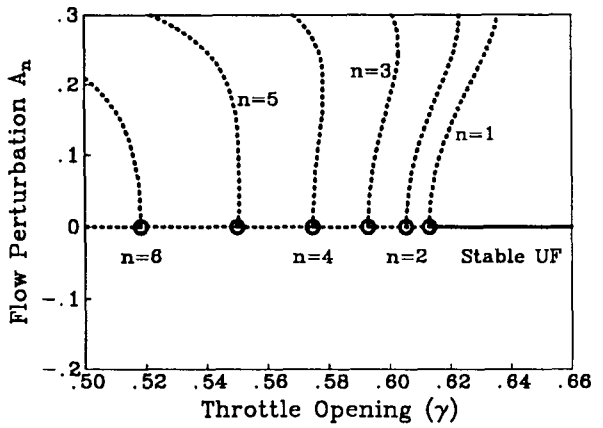

Figure 4: Bifurcating stall modes computed with local methods for $\mu = 0.01$.

bounded maximum positive slope of the compressor characteristic.

While the wave speed is unaffected by this modification, the amplitude expression of the bifurcating stall cells becomes

$$A_n^2 = \frac{8w^3}{3H}\left[\frac{df}{dV} - \mu\frac{n^2}{2\alpha}\right] \tag{15}$$

and the mean gas velocity V of the stalled-flow solutions can be found by:

$$f_0 - \left(\frac{V}{\gamma}\right)^2 - \frac{15HV^2}{2w^2} + \frac{5HV^3}{2w^3} + \frac{6HV}{w} + (V-w)\frac{\mu n^2}{\alpha} = 0. \tag{16}$$

Computing solutions to (16) gives the mean flow values V of the bifurcating stall cells. Note how the roots of (16) are now an explicit function of mode number n, as opposed to the inviscid case (12). In Fig. 4, we observe that the lower mode number stall cells are born during subcritical bifurcations, a signal of possible hysteresis behavior. The nature of the bifurcation changes with larger mode numbers, however, with the $n > 5$ bifurcations being supercritical (with respect to decreasing γ) for the set of parameter values studied.

5. Local Stall Suppression

5.1. 1-D Controllers

In this work we will only consider using the throttle position as a control and so $\gamma = \gamma_0 + u$ is substituted into the plenum mass balance (3). This type of control appears to be simpler to implement than those techniques depending on directly affecting the flow field in the compressor inlet duct[3],[5] and successful experimental results have been reported[4]. An important limitation of this type of control is that is cannot linearly stabilize the bifurcating stall modes: we see that γ does not appear in the linearization of the momentum balance (4) and so this type of control will have no effect on the eigenvalues (6) or (14).

While this control cannot linearly stabilize the uniform flow solution with respect to spatial perturbations, it can improve the operability in the neighborhood of the stall margin. As discussed in the previous section, the subcritical nature of the lower-cell number stall bifurcations leads to operating conditions featuring multistability: conditions where the locally asymptotically stable uniform flow solution coexists with a locally stable fully developed stall cell. Perturbations of the flow field which destabilize the uniform flow operating point correspond to states in the basin of attraction of the stalled flow solutions. The boundaries separating different basins of attraction are the stable manifolds of the smaller amplitude stalled flow solutions with saddle-type stability, born during the stall bifurcations on the uniform flow solution branch. While not directly observable in an experimental system, these unstable equilibria are crucial in organizing the dynamics of the phase space. With this in mind, we see that if the stability of the bifurcating solutions can be controlled, we might be able to improve the compression system's resistance to finite sized disturbances in the neighborhood of the stall margin.

5.2. Bifurcation Control

If we consider the nonlinear state feedback controller of the form[4],[12]

$$\gamma = \gamma_0 + u = \gamma_0 + kA_1^2$$

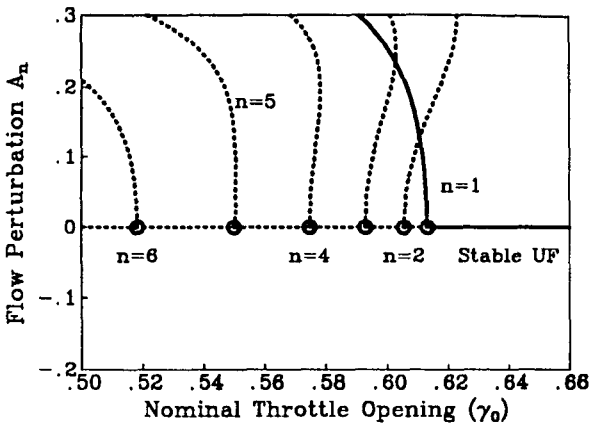

Figure 5: Stabilization of the 1st stall mode with $k = 0.5$.

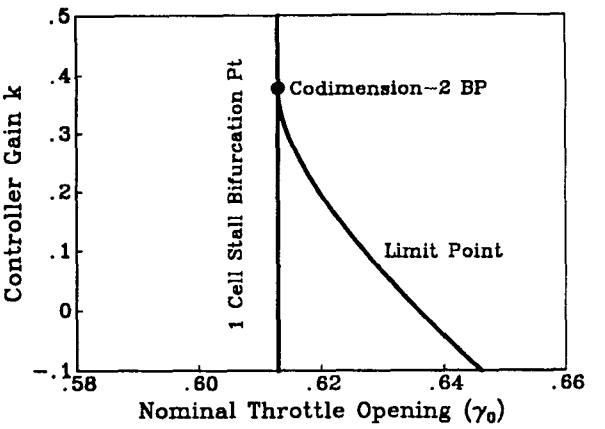

Figure 6: Limit point behavior of the 1st mode as a function of the nonlinear controller gain k.

and compute the stalled flow solutions with the single mode Galerkin discretization, (16) remains valid for $n \geq 2$ while for $n = 1$

$$\left[f_0 - \frac{15HV^2}{2w^2} + \frac{5HV^3}{2w^3} + \frac{6HV}{w} + (V-w)\frac{\mu n^2}{\alpha}\right]\left[\gamma_0 + k\frac{8w^3}{3H}\left(\frac{3HV}{2w^3}(2w-V) - \mu\frac{n^2}{2\alpha}\right)\right]^2 - V^2 = 0. \quad (17)$$

We see that the $[\ldots]^2$ term always reduces to $[\gamma_0]^2$ at the stall bifurcation point, but the roots of (17) away from the stall initiation point will depend on the controller gain k. This is another indication that while the stall point will not be affected by this type of control, the dynamics in the neighborhood will be changed for $k \neq 0$. This can be seen in Fig. 5, where for $k = 0.5$ the single cell stall solution is now born *locally* stable during a supercritical bifurcation (with respect to decreasing throttle opening).

In the uncontrolled system with the single-mode discretization of the axial velocity perturbation, the stalled-flow solution branch, which is unstable near the stall bifurcation point, becomes locally stable at a turning point found at $\gamma_0 \approx 0.636$. If we follow the location of this secondary bifurcation as the controller gain is increased, we find that the value of γ_0 of the limit point and the corresponding amplitude of the stalled-flow solution shrink with increasing k until the limit point and local stall bifurcation points ultimately converge. This marks the transition from subcritical to supercritical bifurcation of the unimodal stalled-flow solution branch in parameter space and takes place at the codimension-2 bifurcation point seen in Fig. 6. For $k > 0.378$, the bifurcating stalled flow solution is locally asymptotically stable and for $k < 0.378$ it is unstable. This means that the controller tuning is a bifurcation problem, which can be solved computationally by computing two-parameter bifurcation diagrams as done here, or by the normal forms approach of Wang and co-workers[12].

5.3. Simulation Results

We have designed and tuned our nonlinear controller using a highly truncated discretization of the flow field perturbation. To test the controller in a more realistic manner, we first assume that the axial velocity perturbation v can be approximated by a higher-order discretization:

$$v = \sum_{n=1}^{N} \exp(n\eta)\left[a_n \cos(n\theta) + b_n \sin(n\theta)\right].$$

Substituting the Fourier expansion into the local momentum balance PDE (13) in a rotating coordinate frame and using Galerkin's method to determine the amplitude coefficients, the $\cos(n\theta)$ moment gives, after some rearranging,

$$\left\{\frac{m}{n} + \frac{1}{\alpha}\right\}\dot{a}_n = \frac{1}{\pi}\int_0^{2\pi} f\cos(n\theta)d\theta - \frac{\mu n^2}{2\alpha}a_n - \left(cm + \frac{cn}{\alpha} + \frac{n}{2\alpha}\right)b_n \quad (18)$$

and the $\sin(n\theta)$ moment gives

$$\left\{\frac{m}{n} + \frac{1}{\alpha}\right\}\dot{b}_n = \frac{1}{\pi}\int_0^{2\pi} f\sin(n\theta)d\theta - \frac{\mu n^2}{2\alpha}b_n + \left(cm + \frac{cn}{\alpha} + \frac{n}{2\alpha}\right)a_n \quad (19)$$

along with the ODEs (2-3). Note that the controller must now take the form $\gamma = \gamma_0 + k(a_1^2 + b_1^2)$. For the results reported in this work, we use $N = 6$.

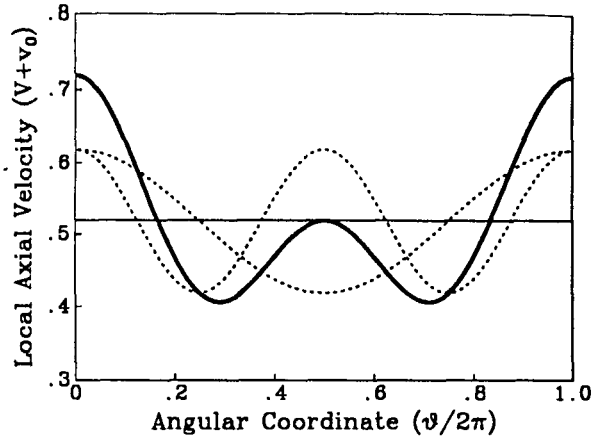

Figure 7: Spatial perturbation (solid curve) introduced to gauge nonlinear stability characteristics of the open/closed-loop system. Dashed curves indicate contributions of individual Fourier modes.

By the local analysis (Fig. 5), the uniform flow solution is locally asymptotically stable to all perturbations (of infinitesimal size) at $\gamma_0 = 0.64$. However, if the axial velocity profile is perturbed in the manner shown in Fig. 7 from the uniform flow equilibrium conditions, and the evolution of this disturbance is followed forward in time, we see that the system settles down to a fully-developed rotating stall equilibrium instead of returning to the uniform flow operating point. This dynamical behavior is shown as the solid curve time trace of Fig. 8, where $V + v_0(\theta = 0)$ is plotted as a function of time. With the nonlinear controller tuned by the local bifurcation analysis techniques discussed in the previous Section, however, the closed-loop system is stable to this perturbation and so returns to the desired uniform flow operating point (see the dashed curves of Fig. 8).

6. Concluding Remarks

From the dynamics of the manipulated parameter shown in Fig. 8, we see that its time scale is on the order of the growth rate of the stall cell amplitude and not on its rotational speed. This means the controller bandwidth demands are reasonable. This makes sense in the context of the "1-dimensional" controls discussed, since the phase of the stall cell is irrelevant in this controller design. This is not the case, of course, for distributed actuators, since they must operate on time scales which are a function of the wave speed and stall cell number.

The stall modes, while uncoupled when the model is linearized, are coupled in a complicated nonlinear fashion (this can be seen explicitly since the integrals of (18-19) can be evaluated by hand with the cubic

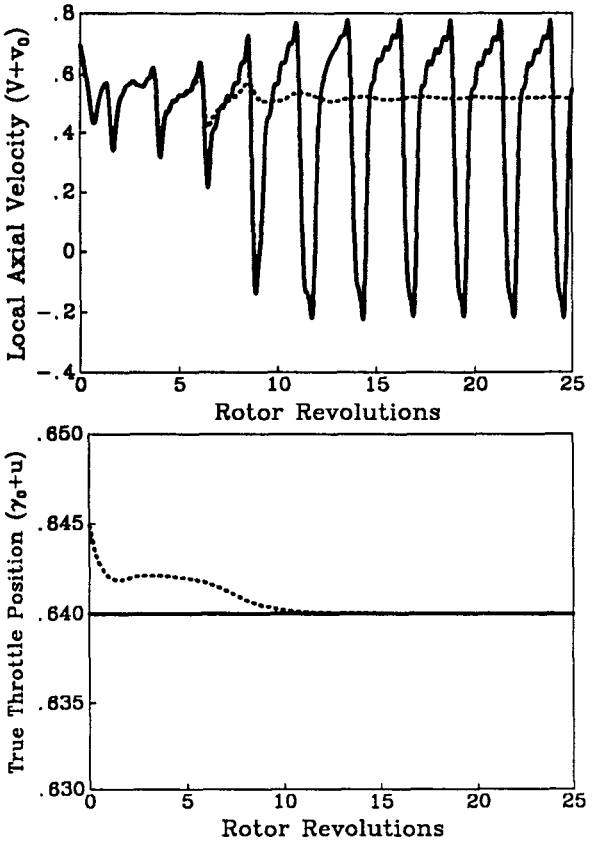

Figure 8: Response to flow perturbations with $k = 0.0$ (solid curve) and $k = 0.5$ (dashed curve)

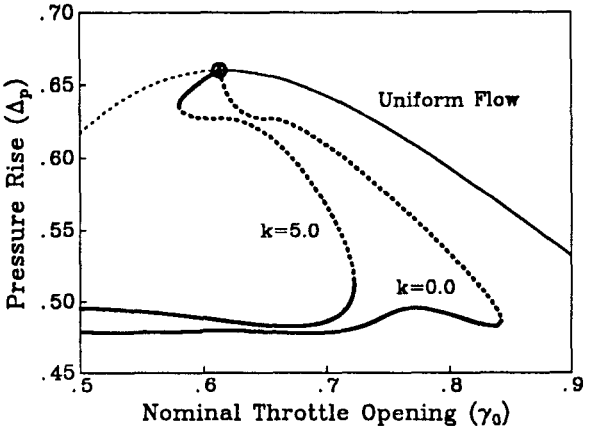

Figure 9: Bifurcation diagrams from which the effects of control on the rotating stall hysteresis loop can be seen. Thicker curves correspond to stalled-flow characteristics.

axisymmetric characteristic used). This means that if the overtones grow quickly, the controller will become ineffective outside the neighborhood of the stall initiation point. Some of these effects can be compensated for by increasing the controller gain, but as seen in Fig. 9, even for a much higher gain than is predicted by local tuning analysis, the bifurcating stalled flow solution becomes unstable giving rise to a hysteresis loop. These bifurcation diagrams were computed with the higher-order discretization ($N = 6$) using a predictor-corrector continuation scheme similar to the algorithm found in the bifurcation analysis package AUTO[13]. While hysteresis is not completely eliminated in this case, the stability of the system to finite sized perturbation in the axial velocity profile is still improved and the range of the hysteresis is also reduced under this control.

This brings up the natural question, presently under investigation, of feedback of higher-frequency modes. Because of the damping effects of viscosity discussed and since the continuum assumption of the model will break down when the period of the stall modes becomes the same length scale of the rotor blades, it is conceivable that a globally stabilizing controller can be found, in principle. The feedback of higher frequency modes is fundamentally important for stall control not only for the stabilization of the unimodal branch, but also for the higher-modal stalled-flow solution branches which do not have any of the lower-frequency components.

7. Acknowledgments

The authors would like to acknowledge the support of the AFOSR through grant F49620-93-1-0186 and by the NSF Engineering Research Centers Program: NSFD CDR-88-03012.

References

[1] Liaw, D. -C., R. A. Adomaitis, and E. H. Abed (1991). Two-parameter bifurcation analysis of axial flow compressor dynamics. *Proc. 1991 American Control Conf.*, Boston.

[2] McCaughan, F. E. (1989). Application of bifurcation theory to axial flow compressor instability. *ASME J. Turbomachinery* **111**, 426-433.

[3] Paduano, J., A. H. Epstein, L. Valavani, J. P. Longley, E. M. Greitzer, and G. R. Guenette (1993). Active control of rotating stall in a low-speed axial compressor. *ASME J. Turbomachinery* **115**, 48-56.

[4] Eveker, K. M. and C. N. Nett (1993). Control of Compression System Surge and Rotating Stall: A Laboratory-Based 'Hands-on' Introduction. Reprint.

[5] Day, I. J. (1993). Active suppression of rotating stall and surge in axial compressors. *ASME J. Turbomachinery* **115**, 40-47.

[6] Badmus, O. O., C. N. Nett, and F. J. Schork (1991). An integrated, full-range surge control/rotating stall avoidance compressor control system. *Proc. 1991 American Control Conf.*, Boston.

[7] Moore, F. K. and E. M. Greitzer (1986). A theory of post-stall transients in axial compression systems: Part 1—Development of equations. *ASME J. of Eng. for Gas Turbines and Power* **108**, 69-76.

[8] Lavrich, P. L. (1988). Time resolved measurements of rotating stall in axial flow compressors. *MIT Gas Turbine Laboratory Report #194.*

[9] Liaw, D. -C. and E. H. Abed (1992). Analysis and control of rotating stall, *Proceedings of NOLCOS'92: Nonlinear Control System Design Symposium*, (M. Fliess, Ed.), Bordeaux, France.

[10] Moore, F. K. and E. M. Greitzer (1986). A theory of post-stall transients in axial compression systems: Part II—Application. *ASME J. of Engineering for Gas Turbines and Power* **108**, 231-239.

[11] Adomaitis, R. A. and E. H. Abed (1993) Bifurcation analysis of nonuniform flow patterns in axial-flow gas compressors. *Proc. 1992 World Cong. Nonlinear Analysts*, Tampa, FL; to appear.

[12] Wang, H. O., R. A. Adomaitis, and E. H. Abed (1993). Active Stabilization of Rotating Stall in Axial-Flow Compressors. *Proc. 1st IEEE Regional Conf. on Aerospace Control Systems*, Thousand Oaks, CA; to appear.

[13] Doedel, E. J. (1981). AUTO: A program for the automatic bifurcation analysis of autonomous systems. *Cong. Num.* **30**, 265-284.